RESEARCH ARTICLE | MARCH 22 2022

An introduction to classical monodromy: Applications to molecules in external fields

Juan J. Omiste ; Rosario González-Férez ; Rafael Ortega

J. Math. Phys. 63, 032702 (2022)
https://doi.org/10.1063/5.0079354

Journal of Mathematical Physics ARTICLE scitation.org/journal/jmp

An introduction to classical monodromy: Applications to molecules in external fields

Cite as: J. Math. Phys. 63, 032702 (2022); doi: 10.1063/5.0079354
Submitted: 20 November 2021 • Accepted: 4 March 2022 •
Published Online: 22 March 2022

Juan J. Omiste,[1,2,a)] Rosario González-Férez,[3,4] and Rafael Ortega[5]

AFFILIATIONS

[1] Departamento de Química Física, Universidad Complutense de Madrid, 28040 Madrid, Spain
[2] Departamento de Química, Universidad Autónoma de Madrid, Módulo 13, Madrid 28049, Spain
[3] Instituto Carlos I de Física Teórica y Computacional and Departamento de Física Atómica, Molecular y Nuclear, Universidad de Granada, 18071 Granada, Spain
[4] ITAMP, Center for Astrophysics | Harvard and Smithsonian, Cambridge, Massachusetts 02138, USA
[5] Departamento de Matemática Aplicada, Universidad de Granada, 18071 Granada, Spain

[a)] **Author to whom correspondence should be addressed:** jomiste@ucm.es

ABSTRACT

An integrable Hamiltonian system presents monodromy if the action-angle variables cannot be defined globally. As a prototype of classical monodromy with azimuthal symmetry, we consider a linear molecule interacting with external fields and explore the topology structure of its phase space. Based on the behavior of closed orbits around singular points or regions of the energy–momentum plane, a semi-theoretical method is derived to detect classical monodromy. The validity of the monodromy test is numerically illustrated for several systems with azimuthal symmetry.

I. INTRODUCTION

Classical monodromy is the topological obstruction to define a global set of action-angle variables in certain integrable classical systems.[1] This phenomenon has crossed the frontiers of mathematics, where it was introduced by Duistermaat[1] and initially considered as a mathematical curiosity with no significant physical applications, to acquire an interdisciplinary interest and popularity in classical and quantum physics. The quantum analog, i.e., quantum monodromy, is the impossibility of assigning a unique set of quantum numbers to characterize all states of a quantum system.[2,3] The existence of monodromy has been proved, both theoretically and experimentally, for a wide variety of classical and quantum systems.

In classical mechanics, the action-angle variables characterize the dynamics of an integrable system and determine the trajectories. Let us highlight that these quantities depend on the topological structure and properties of the phase space. The static manifestation of monodromy, i.e., the absence of global action-angle variables, is a singular fiber in the image of the energy–momentum map as an isolated singular value.[1] The implications of monodromy have been extensively investigated for many classical systems, such as the classical spherical pendulum[2,3] or the champagne bottle potential,[4] among many others. The classical monodromy has been experimentally investigated for the 1:1:2 resonant elastic pendulum, showing that its precession is a multivalued function of the constants of motion.[5] In addition to these static manifestations, the monodromy presents dynamical consequences when a system is continuously driven around a monodromy circuit.[6,7] This dynamical monodromy has been experimentally observed as topological changes on the time-dependent evolution of a spherical pendulum driven by magnetic potentials.[8]

Quantum monodromy appears as a defect in the quantum lattice formed in the energy–momentum by the quantum eigenenergies.[2,3,9] As a consequence, the quantum monodromy significantly influences the spectra of atoms and molecules in external fields[10–12] and even the stability of condensed bosons in optical lattices.[13] Quantum monodromy has been also encountered in the bending spectra of molecules.[14–16] For instance, the bending and symmetric stretching vibrations of the CO_2 molecule[16] provide a molecular realization of the quantum 1:1:2

resonant swing spring.[17] Furthermore, quantum monodromy has been experimentally confirmed in the energy–momentum maps of the end-over-end rotational energy and the two-dimensional bending vibrational energy of cyanogen isothiocyanate molecules[18] and in the bending levels of water molecules.[19] A dynamical manifestation of quantum monodromy has been theoretically explored in terms of topological changes produced in the quantum wave function of the Mexican hat system.[20]

Classical monodromy is, at the present time, a well-developed mathematical theory. For two-degree freedom integrable systems, there are several ways to detect monodromy, for instance, the most recent criteria are linked to the notion of focus–focus singularities.[21] However, the reader can find some difficulties to access this theory since it requires rather sophisticated mathematical tools. The purpose of this paper is to review the origins of the theory and to make it accessible for the non-specialists, aiming at an audience of physicists, theoretical chemists, or general dynamicists.

In this work, we present a semi-theoretical method combining an intuitive description of the family of invariant tori with the numerical computation of an integral. This integral, associated with a winding number, can only take discrete values; therefore, an approximate numerical computation allows us to obtain the exact value. With these elementary tools, we design a method that could be considered insufficient from a strict mathematical point of view but certainly is convincing as a monodromy test. Specifically, we explore the topological features of classical monodromy and apply this monodromy test to a particle whose motion is constrained to the unit sphere and governed by a potential with azimuthal symmetry. Following pioneering works on classical monodromy,[1,2,4] we study the behavior of closed orbits around singular points or regions of the corresponding energy–momentum plane and present a monodromy test to identify and characterize numerically the monodromy of this system. The validity of this test, which is based on the definition of monodromy,[1,2] is illustrated for the unperturbed and perturbed classical spherical pendulums, whose energy–momentum maps are also described.

The analyzed potentials also characterize the rotational dynamics of a linear molecule either in a static electric field[22] or in combined static electric and non-resonant laser fields,[23,24] where the phenomenon of quantum monodromy has been previously analyzed.[12] This numerical study shows that the monodromy test is easily implemented for different potentials and efficiently characterizes the monodromy of a wide variety of systems.

This work is organized as follows: in Sec. II, we describe the dynamical systems under study as well as the topology of the associated space. The phenomenon of monodromy is mathematically analyzed in Sec. III, and an analytical test to determine if a dynamical system presents monodromy is derived. The validity of this monodromy test is illustrated numerically for several systems with azimuthal symmetry in Sec. IV. In Appendixes A and B, we explain some details of the methods and theory discussed in the main text. The main conclusions and perspectives of this work are presented in Sec. V.

II. THE SYSTEM AND ITS TOPOLOGY

The system is formed by a particle of mass $m = 1$, whose motion is constrained to the unit sphere

$$M = T\mathbb{S}^2 = \{(x,p) \in \mathbb{R}^3 \times \mathbb{R}^3 : \| x \| = 1, \langle x,p \rangle = 0\},$$

where x and p stand for the spatial coordinates and the momentum, respectively. The motion of the particle can be described using Lagrangian coordinates $\theta \in [0,\pi]$ and $\varphi \equiv \varphi + 2\pi$ (see Appendix A for more details). As indicated in Appendix A, this chart does not cover the tangent planes at the north and south poles at $\theta = 0$ and $\theta = \pi$, respectively. The particle interacts with a conservative force whose potential is invariant under rotations around the vertical axis, i.e., $V(\theta,\varphi) = V(\theta)$. This potential is an analytic, non-constant, even, and 2π-periodic function, i.e., $V(-\theta) = V(\theta)$ and $V(\theta + 2\pi) = V(\theta)$. Note that throughout this work all functions (in one or several variables) are real analytic. This type of potential describes the interaction of a polar linear molecule with external electric fields parallel to the Z-axis on the laboratory fixed frame. For instance, the potential describing the interaction of a polar molecule with a static electric field[22] is $V(\theta) = \epsilon_1 \cos\theta$, which is the same potential as the classical spherical pendulum. After adding a non-resonant laser to the static electric field, the new potential is[23,24] $V(\theta) = \epsilon_1 \cos\theta + \epsilon_2 \cos^2\theta$. Finally, with a two-color non-resonant laser field, the potential becomes[25] $V(\theta) = \epsilon_1 \cos\theta + \epsilon_2 \cos^2\theta + \epsilon_3 \cos^3\theta$, with ϵ_i, $i = 1,2,3$, being determined by the applied field strengths and the molecular features.

The Hamiltonian of this system reads

$$H = \frac{1}{2}\left(p_\theta^2 + \frac{p_\varphi^2}{\sin^2\theta}\right) + V(\theta),$$

and the equations of motion are

$$\begin{cases} \dot\theta = p_\theta, \quad \dot p_\theta = \dfrac{p_\varphi^2 \cos\theta}{\sin^3\theta} - V'(\theta), \\ \dot\varphi = \dfrac{p_\varphi}{\sin^2\theta}, \quad \dot p_\varphi = 0. \end{cases} \tag{1}$$

Note that due to the azimuthal symmetry, p_φ is an integral of motion. By fixing the energy $H = h$ and the momentum $p_\varphi = j$, the variables θ and φ satisfy

$$\frac{1}{2}\dot{\theta}^2 + V_j(\theta) = h, \tag{2}$$

$$\dot{\varphi} = \frac{j}{\sin^2\theta}, \tag{3}$$

where $V_j(\theta)$ is the modified potential,

$$V_j(\theta) = \frac{j^2}{2\sin^2\theta} + V(\theta),$$

with $V_0(\theta) = V(\theta)$. The energy and momentum are first integrals in involution (in two degrees of freedom, this condition is always satisfied for first integrals), i.e., $\{H, p_\varphi\}_M = 0$, and the Hamiltonian system is Liouville integrable on any region $\Omega \subset M$, satisfying the following: (i) Ω is invariant under the flow (1) and (ii) the differentials $\mathrm{d}H$ and $\mathrm{d}p_\varphi$ are linearly independent on each point of Ω.[26,27] These differentials, which are linear forms on the tangent space at each point of M, can be expressed in terms of the basis $\{\mathrm{d}\theta, \mathrm{d}p_\theta, \mathrm{d}\varphi, \mathrm{d}p_\varphi\}$. The linear independence of $\mathrm{d}H$ and $\mathrm{d}p_\varphi$ is equivalent to saying that the matrix

$$\frac{\partial(H, p_\varphi)}{\partial(\theta, p_\theta, \varphi, p_\varphi)} = \begin{pmatrix} V'(\theta) - \dfrac{p_\varphi^2 \cos\theta}{\sin^3\theta} & p_\theta & 0 & \dfrac{p_\varphi}{\sin^2\theta} \\ 0 & 0 & 0 & 1 \end{pmatrix} \tag{4}$$

has rank two. This is satisfied everywhere, except at the points fulfilling

$$p_\theta = 0, \quad V'(\theta) - \frac{p_\varphi^2 \cos\theta}{\sin^3\theta} = 0, \tag{5}$$

where the rank is 1.

A. Invariant tori

The geometrical and dynamical structure of the sets $\mathcal{S}_{h,j} = \{(\theta, p_\theta, \varphi, p_\varphi) : H = h, p_\varphi = j\}$ depends on the values of j and h. For $j \neq 0$, the modified potential $V_j(\theta)$ diverges as $\theta \to 0^+$ or $\theta \to \pi^-$, i.e., $V_j(\theta) \to \infty$ as $\theta \to 0^+$ or $\theta \to \pi^-$. For a regular value $h > \min_{[0,\pi]} V_j(\theta)$, i.e., $V_j'(\theta) \neq 0$ for each θ such that $V_j(\theta) = h$, Eqs. (2) and (3) describe a finite set of closed trajectories γ_k, with $k = 1, \ldots, r$, in the plane (θ, p_θ). An example is presented in Fig. 1(a) with a prototype potential $V_j(\theta)$, with two closed trajectories, $r = 2$, at $h = 0$. For this potential and

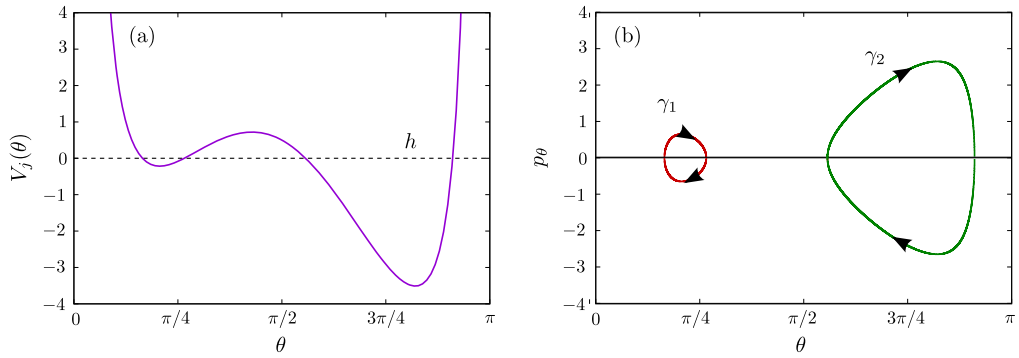

FIG. 1. (a) Modified potential $V_j(\theta) = 2\cos\theta - 5\cos^2\theta + j^2/(2\sin^2\theta)$ with $j = 1$ as a function of θ; the horizontal line represents $h = 0$. (b) Trajectories γ_1 and γ_2 for $h = 0$ in the phase space (θ, p_θ).

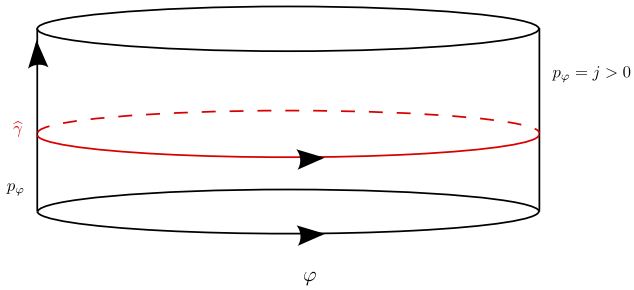

FIG. 2. Phase space (φ, j) for $j > 0$ corresponding to different trajectories $\widehat{\gamma}$.

$h > \min_{[0,\pi]} V_j(\theta)$, there are four turning points, as illustrated in Fig. 1. An example of the trajectories in the phase space is plotted in Fig. 1(b). The orbits γ_k are periodic with the period

$$T_k(h,j) = \sqrt{2}\int_{\alpha_-}^{\alpha_+} \frac{\mathrm{d}\theta}{\sqrt{h - V_j(\theta)}}, \tag{6}$$

where $\alpha_\pm = \alpha_\pm(h,j)$ are the intersection points of the orbit γ_k with the horizontal line $p_\theta = 0$ [see Fig. 1(b)]. In the cylinder (φ, p_φ), the conservation of the angular momentum p_φ and Eq. (3) lead to a closed orbit $\widehat{\gamma} = \{(\varphi, j) : \varphi \in [0, 2\pi]\}$, and an example is given in Fig. 2. For this orbit, the period $\widehat{T}_k = \widehat{T}_k(h,j)$ is implicitly defined by

$$j\int_0^{\widehat{T}_k} \frac{\mathrm{d}t}{\sin^2\theta(t)} = 2\pi, \tag{7}$$

and its orientation is determined by the sign of j. Thus, the set $\mathcal{S}_{h,j}$ is composed by a finite family of invariant tori $\gamma_k \times \widehat{\gamma}$, $k = 1, \ldots, r$. When the periods T_k and $\widehat{T}_k$ are commensurable, for instance, $T_k = 2\sqrt{2}$ and $\widehat{T}_k = 3\sqrt{2}$, then $\theta(t)$ and $\varphi(t)$ have a common period and the invariant torus is foliated with closed orbits. If T_k and $\widehat{T}_k$ are not commensurable, e.g., $T_k = 2\sqrt{2}$ and $\widehat{T}_k = 3$, the orbits lying on the torus are quasiperiodic with frequencies $2\pi/T_k$ and $2\pi/\widehat{T}_k$, respectively.

For $j \neq 0$ and h being a critical value of V_j, the set $\mathcal{S}_{h,j}$ can present different topological configurations. For instance, the potential V_j in Fig. 1 has three critical values $h_1 < h_2 < h_3$, corresponding to three equilibria e_1, e_2, and e_3, respectively. At the minimum $h = h_1$, $\mathcal{S}_{h,j} = \{e_1\} \times \hat{\gamma}$ is homeomorphic to $\mathbb{S}^1$, and at the local minimum $h = h_2$, $\mathcal{S}_{h,j} = (\gamma \times \{e_2\}) \times \hat{\gamma}$, with γ being a closed orbit, it is homeomorphic to the disjoint union of a torus and a circle, $(\mathbb{S}^1 \times \mathbb{S}^1) \vee \mathbb{S}^1$. Whereas at the local maximum $h = h_3$, $\mathcal{S}_{h,j} = E \times \hat{\gamma}$, with E being an eight figure composed by $\{e_3\}$ and two homoclinic connections, and $\mathcal{S}_{h,j}$ is homeomorphic to two tori glued by an equator.

For $j = 0$, i.e., $p_\varphi = 0$, the potential V_0 has no singularities and the trajectories can pass through $\theta = 0$ and $\theta = \pi$, which are the singularities of the parameterization. For this reason, it is convenient to consider the whole plane $(\theta, p_\theta) \in \mathbb{R}^2$ with the identifications $(\theta, p_\theta) \equiv (-\theta, -p_\theta)$, $(\theta + 2\pi, p_\theta) \equiv (\theta, p_\theta)$. Since θ is the latitude on the sphere, this is consistent with the geometry of the problem. After reducing the phase space to the strip $[0, \pi] \times \mathbb{R}$, the orbits touching the vertical lines $\theta = 0$ or $\theta = \pi$ will jump from (θ, p_θ) to $(\theta, -p_\theta)$. For a given regular value h of V, there exists a finite number of closed orbits $\gamma_1, \ldots, \gamma_r$ with energy h. As an example, the closed curves γ_1, γ_2 and $\tilde{\gamma}$ with $r = 2$ and $r = 1$, respectively, are presented in Fig. 3. The geometrical structures of the phase space $(\theta, p_\theta, \varphi, p_\varphi)$ are the invariant tori $\gamma_i \times \{(\varphi, 0) : \varphi \in [0, 2\pi]\}$.

In conclusion, if h is a regular value of V_j, the set $S_{h,j}$ is composed by a finite family of invariant tori for both $j = 0$ and $j \neq 0$.

B. The energy–momentum map

The energy–momentum map is defined as follows:

$$\mathcal{EM} : M \to \mathbb{R}^2, (x,p) \to (H, p_\varphi),$$

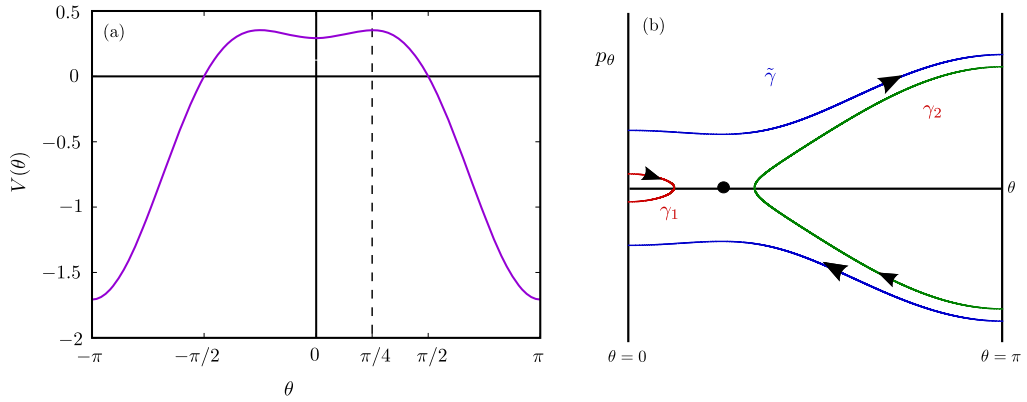

FIG. 3. (a) Potential $V(\theta) = \cos\theta - \frac{\sqrt{2}}{2}\cos^2\theta$ as a function of θ and (b) the orbits γ_1 and γ_2 with h_1 in the interval $V(0) < h_1 < V(\pi/4)$ and $\tilde{\gamma}$ with h_2 satisfying $h_2 > V(\pi/4)$ as a function of θ. The orbit $\tilde{\gamma}$ corresponds to motions through a meridian of the sphere.

and associates an energy–momentum couple to each state. The range of $\mathcal{EM}$ is

$$\mathcal{EM}(M) = \left\{(h,j) \in \mathbb{R}^2 : h \geq \min_{[0,\pi]} V_j\right\}.$$

As expected, this map does not cover the whole $\mathbb{R}^2$ because not all the couples $(h,j) \in \mathbb{R}^2$ are admissible. A point $(h,j) \in \mathbb{R}^2$ is a regular value if the differential of $\mathcal{EM}$ is onto for all the states $(x,p) \in M$ such that $\mathcal{EM}(x,p) = (h,j)$. Otherwise, we say that (h,j) is a singular value. The validity of these definitions is demonstrated by the use of the coordinates $(\theta, p_\theta, \varphi, p_\varphi)$ and the differential of $\mathcal{EM}$ given by the matrix (4). This differential is onto wherever this matrix (4) has rank two. As a consequence, (h,j), with $j \neq 0$, is a regular value of $\mathcal{EM}$ if and only if h is a regular value of V_j, and the same conclusion holds for $j = 0$. The local surjectivity theorem[28] implies that every regular value must be in the interior of $\mathcal{EM}(M)$. Hence, all points (h,j) lying on the boundary of $\mathcal{EM}(M)$ are singular values. Additional singular values can appear in the interior of $\mathcal{EM}(M)$.

C. Action-angle variables: Local theory

Given an invariant torus $\mathcal{T}_0$ such that the differential of $\mathcal{EM}$ has rank two over all the points of $\mathcal{T}_0$, the theorem of Liouville–Arnold[27] allows for a change of variables on a neighborhood of $\mathcal{T}_0$,

$$(x,p) \to (I_1, I_2, \varphi_1, \varphi_2),$$

with $\varphi_i = \varphi_i + 2\pi$, and the form is given by

$$\mathrm{d}\varphi \wedge \mathrm{d}p_\varphi + \mathrm{d}\theta \wedge \mathrm{d}p_\theta = \mathrm{d}\varphi_1 \wedge \mathrm{d}I_1 + \mathrm{d}\varphi_2 \wedge \mathrm{d}I_2.$$

Now, the Hamiltonian only depends on the actions $H = H(I_1, I_2)$, and the equations of motion become

$$\dot{\varphi}_i = \frac{\partial H}{\partial I_i}, \quad \dot{I}_i = 0, \tag{8}$$

with $i = 1, 2$. The phase space is foliated by invariant tori $I_1 = c_1$ and $I_2 = c_2$, which can be also labeled in terms of (h,j), say, $\mathcal{T}_0 = \mathcal{T}_0(h,j)$. This is always the case in a neighborhood of $\mathcal{T}_0 = \mathcal{T}(h_0, j_0)$. The actions are constructed following Arnol'd and Novikov.[29] First, two oriented loops

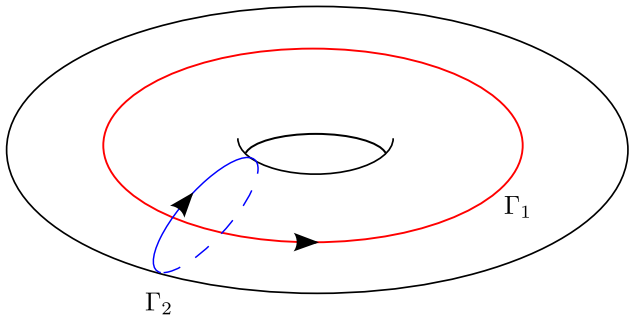

FIG. 4. Oriented loops $\Gamma_1(h,j)$ and $\Gamma_2(h,j)$ in the invariant tori $\mathcal{T} = \mathcal{T}(h,j)$.

$\Gamma_1(h,j)$ and $\Gamma_2(h,j)$ are selected in $\mathcal{T}(h,j)$ to generate the first homology group of the torus in Fig. 4. These loops must be chosen so that they depend continuously on (h,j). The actions are computed via the integrals

$$I_i = \frac{1}{2\pi}\int_{\Gamma_i}(p_\theta \mathrm{d}\theta + p_\varphi \mathrm{d}\varphi). \tag{9}$$

Let us consider a domain $G^+ \subset \{j > 0\}$, which is fibered by invariant tori and is small enough, so that the Liouville–Arnold theorem is applicable. Assume that $\gamma = \gamma(h,j)$ is a closed orbit of Eq. (2), which depends analytically on (h,j). Assuming that γ is the projection of $\mathcal{T}(h,j)$ on the plane (θ, p_θ), the loops are defined as

$$\Gamma_1(h,j) = \gamma(h,j) \times \{(\pi, j)\}, \quad \Gamma_2(h,j) = \{(\theta^*, p_\theta^*)\} \times \widehat{\gamma},$$

where (θ^*, p_θ^*) is a point in γ and $\widehat{\gamma} = \widehat{\gamma}(j) = \{(\varphi, j) : \varphi \in [0, 2\pi]\}$. Combining this definition with Eq. (9), it yields

$$\begin{cases} I_1 = \dfrac{1}{2\pi}\displaystyle\int_{\Gamma_1} p_\theta \mathrm{d}\theta = \frac{1}{\pi}\int_{\alpha_-}^{\alpha_+} \sqrt{2(h - V_j(\theta))}\mathrm{d}\theta, \\ I_2 = \dfrac{1}{2\pi}\displaystyle\int_{\Gamma_2} p_\varphi \mathrm{d}\varphi = j, \end{cases} \tag{10}$$

where $\alpha_\pm = \alpha_\pm(h,j)$ are the points of γ lying on the horizontal axis $p_\theta = 0$ satisfying $V_j(\alpha_\pm) = h$. The value of α_+ will be 0 (respectively, π) when γ does not intersect $p_\theta = 0$ by the left (respectively, by the right). The action $I_1 = I_1(h,j)$ is analytic on G^+. The actions can analogously be defined on the symmetric domain $G^- \subset \{j < 0\}$.

It is interesting to discuss the behavior of the points $\alpha_\pm$ as $j \to 0$ and $h \to h_0$. Assuming that $\gamma(h,j)$ converges to a closed orbit $\gamma(h_0, 0)$, where h_0 is a regular value of V_0 with $\min V_0 < h_0 < \max V_0$, then

$$\lim_{(h,j)\to(h_0,0)} \alpha_\pm(h,j) = \alpha_\pm(h_0,0)$$

with $0 \le \alpha_-(h_0,0) < \alpha_+(h_0,0) \le \pi$.

For $h_0 > \max V_0$, the orbit $\gamma(h,j)$ converges to the closed curve composed by the arcs $\tilde{\gamma}$ and two segments of the lines $\theta = 0$ and $\theta = \pi$ (see Fig. 3). As a consequence,

$$\lim_{(h,j)\to(h_0,0)} \alpha_-(h,j) = 0, \qquad \lim_{(h,j)\to(h_0,0)} \alpha_+(h,j) = \pi.$$

D. Action-angle variables: Global aspects

The action-angle variables are quite rigid, and this implies that their global definition requires a deeper analysis. Given a domain $D \subset M$ invariant under the Hamiltonian flow, action-angle variables can be defined on D if there is a symplectic diffeomorphism,

$$\psi : D \subset M \to D_1 \subset \mathbb{R}^2 \times \mathbb{S}^1 \times \mathbb{S}^1, \quad (x,p) \to (I_1, I_2, \varphi_1, \varphi_2)$$

with $H = H(I_1, I_2)$. Given two systems of action-angle $\psi : D \to D_1$ and $\widetilde{\psi} : \widetilde{D} \to \widetilde{D}_1$, there exists a 2×2 matrix A, with constant integer entries and $\det A = 1$ and a constant vector $c \in \mathbb{R}^2$, such that the actions in the two systems satisfy

$$\begin{pmatrix} I_1 \\ I_2 \end{pmatrix} = A \begin{pmatrix} \widetilde{I}_1 \\ \widetilde{I}_2 \end{pmatrix} + c \tag{11}$$

on $D \cap \widetilde{D}$. This is valid for any integrable Hamiltonian system such that the frequencies of the invariant tori, $\omega_i = \frac{\partial H}{\partial I_i}$ with $i = 1, 2$, are $\mathbb{Z}$-linearly independent and this holds for almost all tori.[27] For the systems considered in this work, this is equivalent to say that the periods of $\theta(t)$ and $\varphi(t)$, $T(h,j)$ in Eq. (6) and $\widehat{T}(h,j)$ in Eq. (7), are not commensurable for most (h,j). This is satisfied because the ratio $T(h,j)/\widehat{T}(h,j)$ is not constant. Indeed, if $(h,j) \to (h_0, 0)$, with h_0 being a regular value of V_0 and $\min V_0 < h_0 < \max V_0$, then $T(h,j)$ tends to a positive number, whereas $\widehat{T}(h,j)$ diverges to infinity.

III. MONODROMY

In the plane (h,j), we consider a circuit C contained in the region of regular values of $\mathcal{EM}$, which crosses the line $j = 0$ at two points $h = a$ and b and encircles a singular value lying on the line $j = 0$ (see Fig. 5). Associated to this circuit, there is a family of invariant tori $\mathcal{T} = \mathcal{T}(h,j)$, $(h,j) \in C$, depending continuously on (h,j). This circuit admits a system of action-angle variables defined in the domain D if there is a sympletic diffeomorphism ψ satisfying the conditions given in Sec. II D, and the domain D contains all invariant tori $\mathcal{T}(h,j)$. Note that it would be more precise to say that the family of invariant tori $\mathcal{T}$ admits these coordinates. The Hamiltonian system possesses monodromy if some circuit in $\mathcal{EM}$ does not admit action-angle coordinates.[1]

To derive a semi-theoretical method to detect monodromy, it will be assumed that the family of invariant tori $\mathcal{T}$ is of the first kind described in Sec. II A. This means that for each $(h,j) \in C$, the invariant torus $\gamma(h,j) \times \hat{\gamma}$ is such that $h > \min V_j$ is a regular value of the modified potential and $h < \max V_0$ if $j = 0$. In particular, it holds

$$0 < \alpha_-(h,j) < \alpha_+(h,j) < \pi, \quad (h,j) \in C, \ j \neq 0. \tag{12}$$

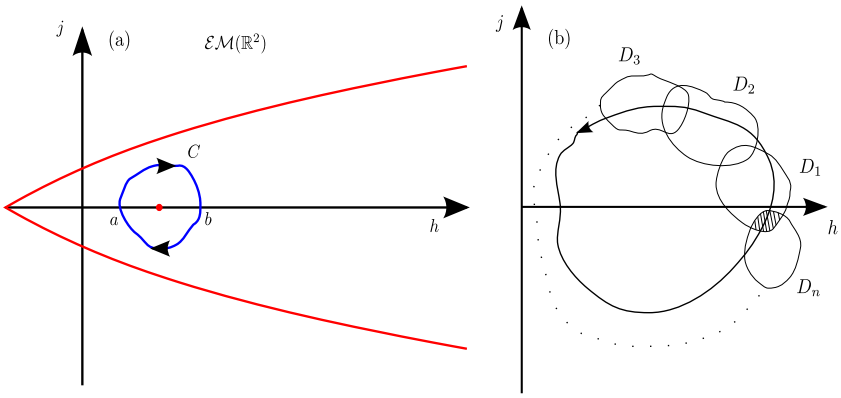

FIG. 5. (a) Circuit C around a singular value in the line $j = 0$ in the plane (h,j) contained in the region of regular values of $\mathcal{EM}$ and (b) example of a family of domains D_k covering the contour C.

The remaining cases can be treated similarly. For each (h,j) with $j \neq 0$, we define the function

$$\chi(h,j) = -\frac{j}{\pi}\int_{\alpha_-}^{\alpha_+} \frac{1}{\sqrt{2(h - V_j(\theta))}} \frac{\mathrm{d}\theta}{\sin^2\theta}. \tag{13}$$

The integrand has a singularity at $\theta = \alpha_\pm$, which is of the order of $|\theta - \alpha_\pm|^{-1/2}$, and therefore, the integral is finite.

At the point $(a,0)$, which lies in the intersection of the circuit and the line $j = 0$, we define

$$\Delta(a,0) = \lim_{\substack{(h,j)\to(a,0)\\ j>0}} 2\chi(h,j). \tag{14}$$

We will prove that this limit always exists and it takes integer values. Analogously, $\Delta(b,0)$ is defined at the point $(b,0)$, which also takes integer values. The criterion for the existence of monodromy along the circuit C is

$$\Delta(a,0) \neq \Delta(b,0). \tag{15}$$

To justify these statements, let us go back to the definition of action variables in Eq. (10). They are well defined in a small neighborhood of $C_+ = C \cap \{j > 0\}$ or $C_- = C \cap \{j < 0\}$. The Jacobian matrix of $I = (I_1, I_2)$ can be computed in each of these two regions,

$$DI(h,j) = \begin{pmatrix} \beta & \chi \\ 0 & 1 \end{pmatrix},$$

with

$$\beta = \beta(h,j) = \frac{1}{\pi}\int_{\alpha_-}^{\alpha_+} \frac{\mathrm{d}\theta}{\sqrt{2(h - V_j(\theta))}}. \tag{16}$$

Note that there are not additional terms involving the derivatives of $\alpha_\pm(h,j)$ because $V(\alpha_\pm) = h$. Since $\beta > 0$, $DI(h,j)$ has an inverse for $j \neq 0$, and it is straightforward to show that $\beta(h,-j) = \beta(h,j), \chi(h,-j) = -\chi(h,j)$ and

$$DI(h,j)DI(h,-j)^{-1} = \begin{pmatrix} 1 & 2\chi(h,j) \\ 0 & 1 \end{pmatrix}. \tag{17}$$

Let us now prove that the limit defining $\Delta(a,0)$ in Eq. (14) really exists, and it is an integer number, which also holds for $\Delta(b,0)$. The Liouville–Arnold theorem can be applied at the invariant torus $\mathcal{T}(a,0)$. The local action-angle variables are defined on some open set $D_a \subset M$ with $\mathcal{T}(a,0) \subset D_a$. The continuity of the family of tori allows us to find a neighborhood of $(a,0)$, $\mathcal{U} \subset \mathcal{EM}$, such that

$$\mathcal{T}(h,j) \subset D_a \qquad \text{if} \quad (h,j) \in \mathcal{U}. \tag{18}$$

The corresponding actions, denoted by $\widetilde{I}_1$ and $\widetilde{I}_2$, are smooth functions of $(h,j) \in \mathcal{U}$. The actions I_1 and I_2, given by Eq. (10), are also smooth functions of (h,j), but they are defined in a region of $\{j > 0\}$, more precisely, in a neighborhood D_+ of $C \cap \{j > 0\}$, as shown in Fig. 6. According to Eq. (11), in the common region $D_+ \cap \mathcal{U}$, it holds

$$DI(h,j) = A_+ D\widetilde{I}(h,j), \tag{19}$$

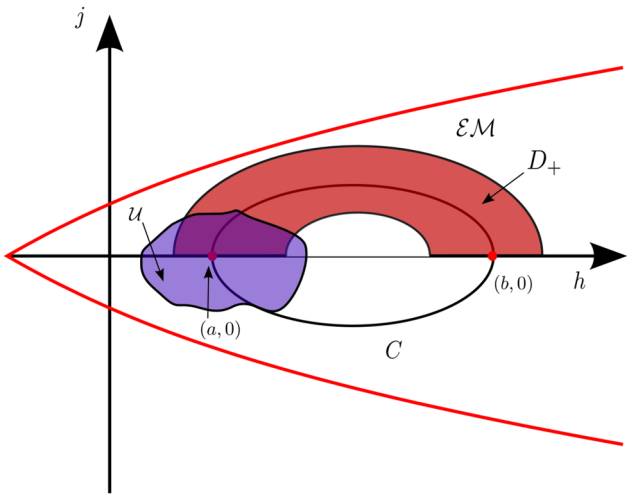

FIG. 6. Domain D_+ in a neighborhood of $C \cap \{j > 0\}$, and neighborhood of $(a,0)$, $\mathcal{U}$, in which the actions $\widetilde{I}_1$ and $\widetilde{I}_2$ are smooth functions of (h,j).

where A_+ is a matrix in the unimodular group, i.e., it has integer entries and $\det A_+ = 1$. Since $\widetilde{I}(h,j)$ is a smooth function in a neighborhood of $(a,0)$, the limit

$$DI(a,0^+) := \lim_{\substack{(h,j)\to(a,0)\\ j>0}} DI(h,j) = A_+ D\widetilde{I}(a,0) \tag{20}$$

exists. Furthermore, since $\chi(h,j)$ is one of the entries of the matrix $DI(h,j)$, the limit $\Delta(a,0)$ in Eq. (14) also exists.

Working on $\{j < 0\}$, we obtain another limit,

$$DI(a,0^-) = A_- D\widetilde{I}(a,0) \tag{21}$$

with A_- being another unimodular matrix. In consequence,

$$DI(a,0^+)DI(a,0^-)^{-1} = A_+ A_-^{-1}, \tag{22}$$

and from Eq. (17),

$$DI(a,0^+)DI(a,0^-)^{-1} = \begin{pmatrix} 1 & \Delta(a,0) \\ 0 & 1 \end{pmatrix}. \tag{23}$$

Since the matrix $A_+A_-^{-1}$ is unimodular, the entry $\Delta(a,0)$ must be an integer. The previous discussion is also applicable at the point $(b,0)$, obtaining that $\Delta(b,0)$ is also a well-defined integer.

Let us now explain why $\Delta(a,0) \neq \Delta(b,0)$ implies monodromy. In the absence of it, there should exist a global system of action-angle coordinates. This means that there exists a diffeomorphism ψ, satisfying the conditions of Sec. II C, defined on a domain D containing the whole family of invariant tori, $\mathcal{T}(h,j) \subset D$, for each $(h,j) \in C$. The action variables associated with this system, $\mathcal{I}_1$ and $\mathcal{I}_2$, are smooth functions of (h,j), $\mathcal{I}_i = \mathcal{I}_i(h,j)$, and defined on some neighborhood of C, say, $\mathcal{V} \subset \mathcal{EM}$ (see Fig. 7). By previous arguments, we know that there are unimodular matrices, again denoted by $A_\pm$, and it holds

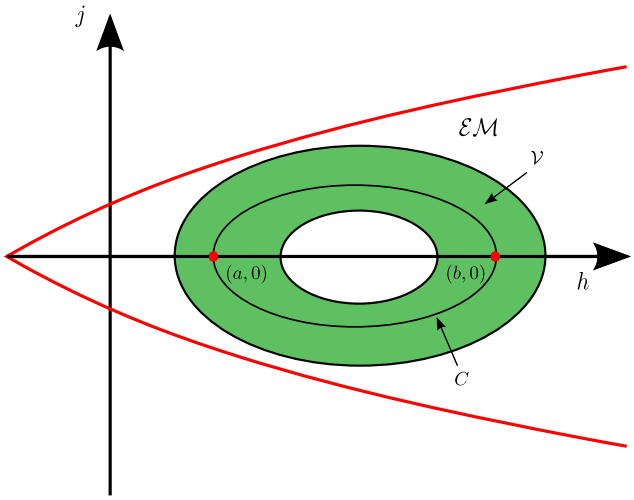

FIG. 7. Neighborhood of C, $\mathcal{V}$, where the action variables $\mathcal{I}_i = \mathcal{I}_i(h,j)$, with $i = 1, 2$ being defined.

$$DI(h,j) = A_+ D\mathcal{I}(h,j) \quad \text{on} \quad \mathcal{V} \cap D_+, \tag{24}$$
$$DI(h,j) = A_- D\mathcal{I}(h,j) \quad \text{on} \quad \mathcal{V} \cap D_-. \tag{25}$$

Then, it yields

$$DI(a,0^+)DI(a,0^-)^{-1} = \lim_{\substack{(h,j)\to(a,0)\\ j>0}} A_+ D\mathcal{I}(h,j) D\mathcal{I}(h,-j)^{-1} A_-^{-1}. = A_+ A_-^{-1}. \tag{26}$$

Since the same argument applies at the point b, obtaining

$$DI(b,0^+)DI(b,0^-)^{-1} = A_+ A_-^{-1}, \tag{27}$$

this implies that $\Delta(a,0) = \Delta(b,0)$. In conclusion, the existence of monodromy can be confirmed by numerically checking that $\Delta(a,0) \neq \Delta(b,0)$, which means that a global system of action-angle coordinates cannot be defined.[1]

IV. NUMERICAL EVALUATION OF MONODROMY

This section is devoted to illustrate the validity of the monodromy test by applying it to several physical systems, which are known to present the phenomenon of monodromy. The generic potential for these systems is given by

$$V(\theta) = -\omega \cos\theta - \eta \cos^2\theta - \lambda \cos^3\theta, \tag{28}$$

with $\lambda, \eta, \omega \in \mathbb{R}$.

As a first example, we consider the classical spherical pendulum, $V(\theta) = -\omega \cos\theta$, with $\omega > 0$ and $\lambda = \eta = 0$, equivalent to $V(\theta) = \omega \cos\theta$. This potential also describes the interaction of a polar rigid molecule with a static electric field parallel to the Z axis of the laboratory fixed frame with $\omega = d\epsilon$, with d being the permanent electric dipole moment of the molecule and ϵ being the electric field strength.[22] Equation (5) for the singular points, with the change of coordinate $x = \cos\theta$, reads

$$\omega(1-x^2)^2 - j^2 x = 0. \tag{29}$$

This equation has exactly one root lying in the interval $[-1,1]$ for $j \neq 0$ and the roots ± 1 for $j = 0$. The singularities on the energy–momentum region $\mathcal{EM}$ are the isolated point $(\omega, 0)$ and the boundary, described by the curve of equation $h = \frac{j^2}{2(1-x(j)^2)} - \omega x(j)$, where $x(j)$ is the root of Eq. (29) lying in $[-1,1]$. The $\mathcal{EM}$ map is presented in Fig. 8(a), where ω has been fixed to $\omega = 1$ without loss of generality. Let us consider the family of invariant tori through a path in $\mathcal{EM} \cap \{j \geq 0\}$ connecting the points $(a,0)$ and $(b,0)$ with $-\omega < a < \omega < b$ indicated in Fig. 8(a). Specifically, we choose three tori along this path and present their projections on the plane (θ, p_θ) in Fig. 8(b). As we observe, these trajectories smoothly connect the cases at each side of the singularity $(\omega, 0)$, that is to say, open at $\theta = 0$ and open at $\theta = 0$ and π for $(a,0)$ and $(b,0)$, respectively.

Figure 8(c) shows $\chi(h,j)$ as a function of j for several values of h. In Appendix B, the numerical procedure to compute the integral $\chi(h,j)$ is explained. For $h > 1$, it holds $\lim_{j\to 0^+}\chi(h,j) = -1$, whereas for $h < 1$, $\lim_{j\to 0^+}\chi(h,j) = -1/2$. Thus, the inequality in Eq. (15) is satisfied

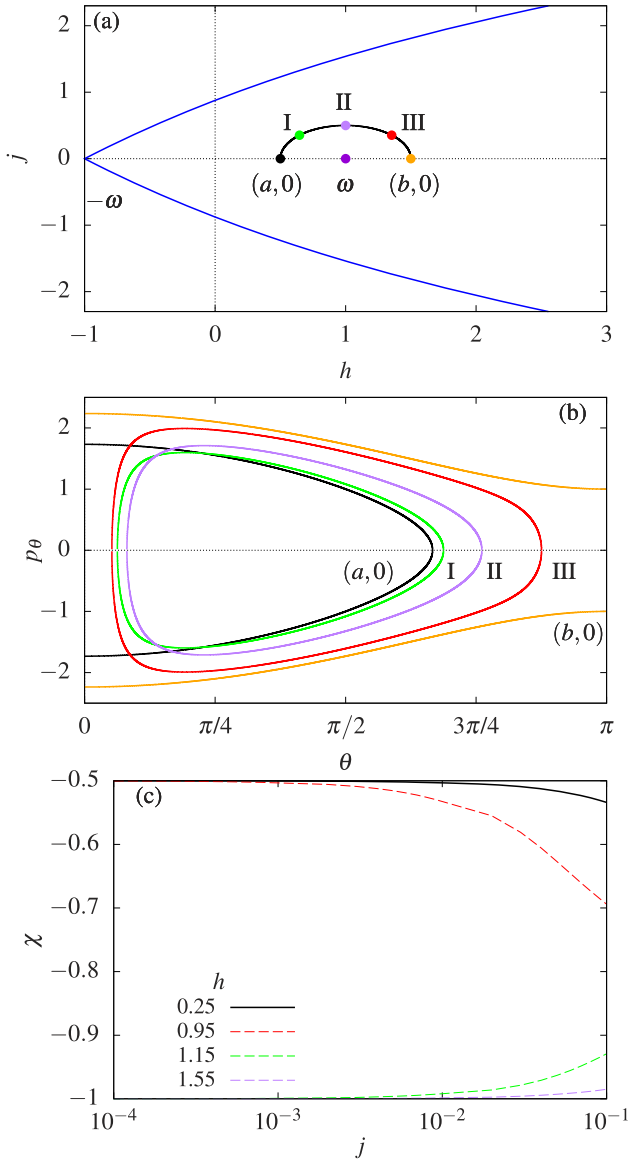

FIG. 8. Spherical pendulum with $\omega = 1$: (a) the energy–momentum plane $\mathcal{EM}$ and tori I $= (1 - \frac{\sqrt{2}}{4}, \frac{\sqrt{2}}{4})$, II $= (1, \frac{1}{2})$, and III $= (1 + \frac{\sqrt{2}}{4}, \frac{\sqrt{2}}{4})$ (full points) along a path connecting $(a,0) = (\frac{1}{2}, 0)$ and $(b,0) = (\frac{3}{2}, 0)$ around the singular point $(0,\omega)$; (b) projections of the tori on the plane (θ, p_θ); and (c) $\chi(h,j)$ as a function of j for several values of h.

because

$$\left[\Delta(b,0^+) - \Delta(a,0^+)\right] = -1, \tag{30}$$

with $-1 < a < 1$ and $b > 1$, which indicates the existence of monodromy.

The next system is a perturbed classical spherical pendulum $V(\theta) = -\omega\cos\theta - \eta\cos^2\theta$, with $\omega, \eta < 0$ and $\omega > 2\eta$. Using again as coordinate $x = \cos\theta$ and assuming $\theta \neq 0, \pi$, the singular-point equation (5) reads

$$(\omega + 2\eta x)(1 - x^2)^2 - j^2 x = 0. \tag{31}$$

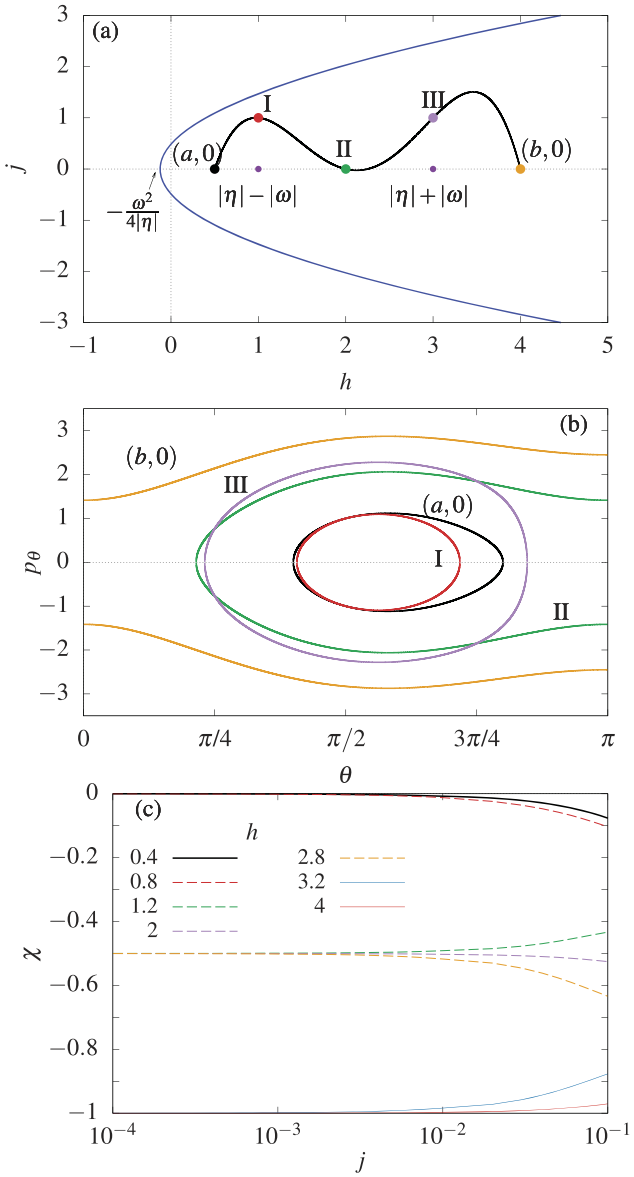

FIG. 9. Modified spherical pendulum with $\omega = -1$ and $\eta = -2$: (a) the energy–momentum plane $\mathcal{EM}$ and tori I = (1, 1), II = (2, 0), and III = (3, 1) (full points) along a path connecting $(a, 0) = (0.5, 0)$ and $(b, 0) = (4, 0)$; (b) projections of the tori on the plane (θ, p_θ); and (c) $\chi(h, j)$ as a function of j for several values of h.

The computations show that this equation possesses only one solution for $j \neq 0$ lying in $[-1, 1]$, whereas for $j = 0$, there are three roots lying in $[-1, 1]$ with values $\pm 1, -\frac{\omega}{2\eta}$. Thus, the singularities on $\mathcal{EM}$ for this potential are two isolated points and the boundary, with the equation $h = \frac{j^2}{2(1-x(j)^2)} - \omega x(j) - \eta x(j)^2$, where $x(j) \in [-1, 1]$ is the root of Eq. (31). Specifically, the singular points for $j = 0$ are $-\omega - \eta = |\eta| + |\omega|$, $\omega - \eta = |\eta| - |\omega|$, and $\frac{\omega^2}{4\eta} = -\frac{\omega^2}{4|\eta|}$, which is included in the boundary. The $\mathcal{EM}$ map is presented in Fig. 9(a). The points $|\eta| \pm |\omega|$ are the candidates to be the monodromy points, which are 1 and 3 for $\omega = -1$ and $\eta = -2$, respectively. Monodromy is illustrated along a path connecting three tori lying on the $j = 0$ axis [see Fig. 9(a)]. The projections on the (p_θ, θ) plane of the three tori I, II, and III are closed, open on one side, and open on both sides, respectively, as shown in Fig. 9(b). For several values of the total energy h, Fig. 9(c) illustrates the evolution of $\chi(h, j)$ as j decreases. It holds $\lim_{j\to 0^+}\chi(h, j) = 0$ for $0 < h < 1$, $\lim_{j\to 0^+}\chi(h, j) = -0.5$ for $1 < h < 3$, and $\lim_{j\to 0^+}\chi(h, j) = -1$ for

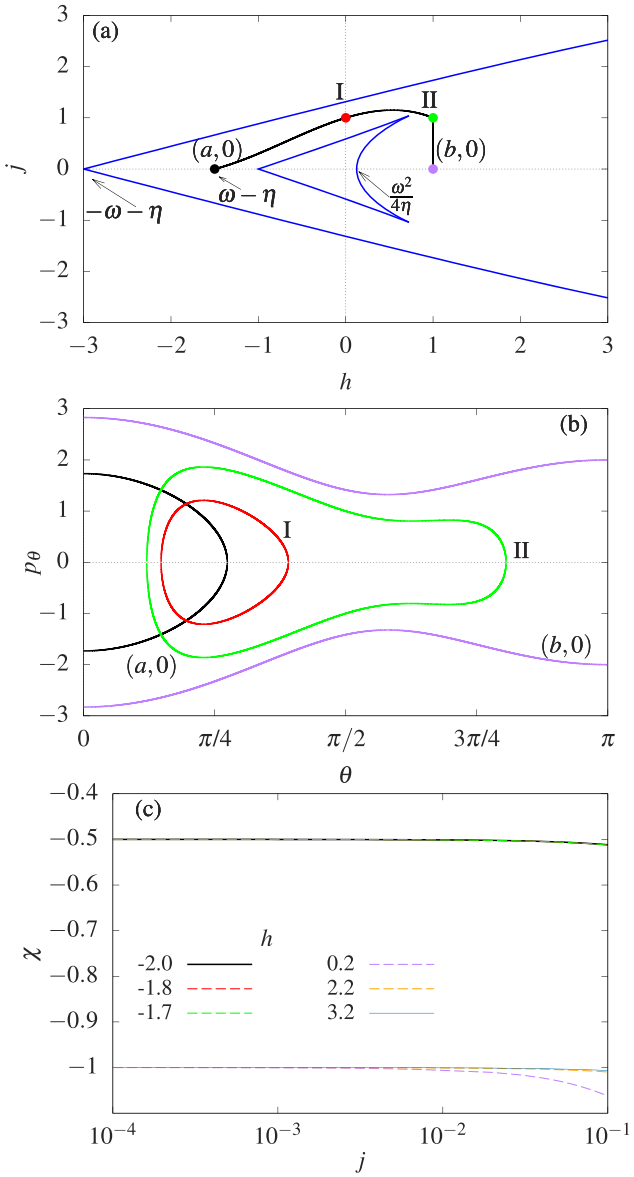

FIG. 10. Modified spherical pendulum with $\omega = 1$ and $\eta = 2$: (a) the energy–momentum plane $\mathcal{EM}$ and tori I $= (0, 1)$ and II $= (1, 1)$ (full points) along a path connecting $(a, 0) = (-1.5, 0)$ and $(b, 0) = (1, 0)$; (b) projections of the tori on the plane (θ, p_θ); and (c) $\chi(h, j)$ as a function of j for several values of h.

$h > 3$. As a consequence, for a closed trajectory containing one or two monodromy points, the inequality (15) is satisfied, and therefore, monodromy exists.

By considering the parameters $\omega, \eta > 0$, this potential $V(\theta) = -\omega\cos\theta - \eta\cos^2\theta$ describes the interaction of a polar rigid molecule with a static electric field and a non-resonant laser field,[23,24] both parallel to the Z axis, with $\omega = d\epsilon$ and $\eta = I\Delta\alpha/2c\epsilon_0$, where $\Delta\alpha$ is the polarizability anisotropy, I is the laser intensity, c is the speed of light, and ϵ_0 is the dielectric constant. For $\omega < 2\eta$, the singular-point equation (5), with $x = \cos\theta$, is given by

$$(\omega + 2\eta x)(1 - x^2)^2 - j^2 x = 0. \tag{32}$$

For this potential, the singularities are $-\eta - \omega$, $-\eta + \omega$, and $\omega^2/4\eta$; whereas Eq. (32) has one, two or three roots for $j \neq 0$. Thus, the set of regular values of $\mathcal{EM}$ has two connected components, as illustrated in Fig. 10(a). For the invariant tori in Fig. 10(a), we present in Fig. 10(b) their projections on the (θ, p_θ) plane. For $\omega = 1$, $\eta = 2$, and several values of h, the numerical results for $\chi(h, j)$ are presented as a function of j in Fig. 10(c). The limits $\lim_{j\to 0^+}\chi(h > \frac{\omega^2}{4\eta}, j)$ and $\lim_{j\to 0^+}\chi(h < \omega - \eta, j)$, taken from the right or left side of the inner region, respectively, are different confirming the existence of monodromy in this system.

As a last example, we consider the general potential (28), which represents the interaction of a diatomic polar molecule in a two-color non-resonant laser field.[25] The parameters are $\eta = \frac{1}{4}\Delta\alpha(\epsilon_1^2 + \epsilon_2^2)$, $\lambda = \frac{1}{8}\Delta\beta\epsilon_1^2\epsilon_2\cos(2\delta_2 - \delta_1)$, and $\omega = \frac{3}{8}\beta_\perp\epsilon_1^2\epsilon_2\cos(2\delta_2 - \delta_1)$, with $\beta_\perp$ and $\Delta\beta$ being the hyperpolarizability perpendicular component and anisotropy, respectively, and $\epsilon_{1,2}$ and $\delta_{1,2}$ are the field strengths and phases of the two components of the laser field, respectively. The condition equation (5) reads

$$\left[2\eta x + 3\lambda x^2 + \omega\right](1 - x^2)^2 - j^2 x = 0, \tag{33}$$

where $x = \cos\theta$. For $j = 0$, the regularization condition (33) is fulfilled for $x = \pm 1$ and $x = \frac{1}{3\lambda}\left(-\eta \pm \sqrt{\eta^2 - 3\lambda\omega}\right)$. Thus, for $3\lambda\omega > \eta^2$, we encounter the roots $x = \pm 1$, with energy values $h = \mp\lambda - \eta \mp \omega$, respectively. In addition to these two roots, a third one, $x = -\frac{\eta}{3\lambda}$, appears for $3\lambda\omega = \eta^2$ and two more, $x = \frac{1}{3\lambda}\left(-\eta \pm \sqrt{\eta^2 - 3\lambda\omega}\right)$ for $3\lambda\omega < \eta^2$. Here, we are assuming that the parameters ω, η, and λ satisfy the appropriate conditions so that the roots are in the interval $x \in [-1, 1]$.

Due to the complexity of the roots, we only present the results for the parameters $\lambda = -1.1$, $\eta = -0.2$, and $\omega = 1.2$. The roots are $x = \pm 1$, $x \approx 0.5455$, and $x \approx -0.6667$, having the Hamiltonian the values $h = 0.1, 0.3, -0.4165$, and 0.5630, respectively. To illustrate this system, Fig. 11 shows the interaction potential for $j = 0$. For $h \leq -0.4165$, the system does not present orbits, since the kinetic energy cannot be larger than 0. A unique type of orbit is found for $-04\,165 < h < 0.1$; in this case, the values of θ are restricted to the left well. By increasing the energy to $0.1 < h < 0.3$, there is still one type of orbit; however, the system is able to access $\theta = 0$. Due to the potential barrier for $0.3 < h < 0.563$, there are two regions in the phase space containing orbits. If the energy of the system is larger than the potential maximum located around $3\pi/4$, i.e., $h > 0.563$, the orbits cover the whole space.

The corresponding $\mathcal{EM}$-map is presented in Fig. 12(a), where an irregular point and an irregular curve are observed. An example path around these irregular point and curve is also shown in this figure. The projections on the (θ, p_θ) plane of these invariant tori are plotted in Fig. 12(b), where we observe all kind of trajectories. As in the previous cases, the limit $\lim_{j\to 0^+}\chi(h, j)$, presented in Fig. 12(c), depends on the value of h. We obtain $\lim_{j\to 0^+}\chi(h, j) = -1, -0.5$, and 0 for $-0.4165 < h < 0.1$, $0.1 < h < 0.3$, and $h > 0.563$, respectively, which proves the existence of monodromy.

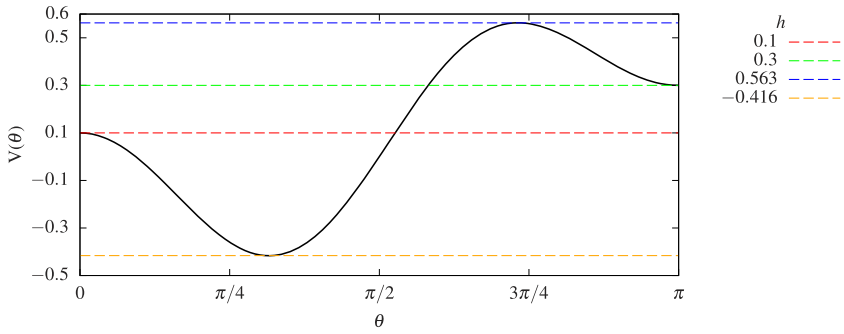

FIG. 11. Interaction potential $V(\theta) = 1.1\cos^3\theta + 0.2\cos^2\theta - 1.2\cos\theta$: the horizontal lines represent the energies at the singular points at $j = 0$.

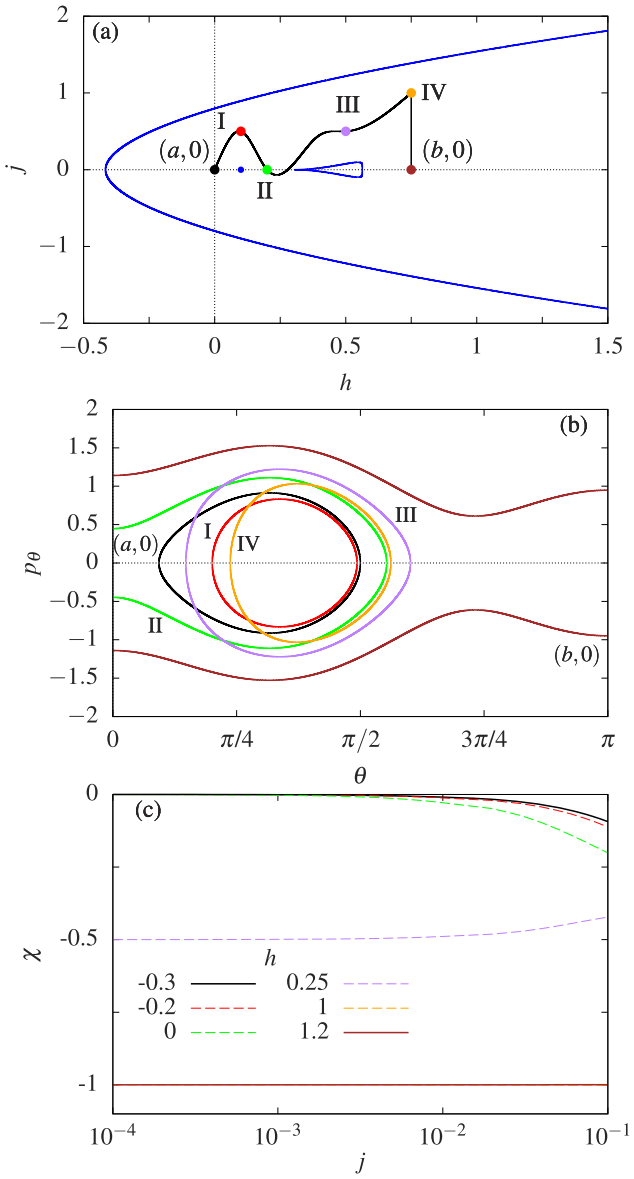

FIG. 12. Modified spherical pendulum with $\omega = 1.2$, $\eta = -0.2$, and $\lambda = -1.1$: (a) the energy–momentum plane $\mathcal{EM}$ and tori I = (0.1, 5), II = (0.2, 0), III = (0.5, 0.5), and IV = (0.75, 1) (full points) along a path connecting $(a, 0) = (0, 0)$ and $(b, 0) = (0.75, 0)$; (b) projections of these tori on the plane (θ, p_θ); and (c) $\chi(h, j)$ as a function of j for several values of h.

V. CONCLUSIONS

We have considered a particle whose motion is constrained to the unit sphere and governed by an external potential having azimuthal symmetry. For this system, the topology and the local and global angle-action variables are explored in detail. The monodromy in a system appears if the angle-action variables are impossible to define globally. In this work, we have presented a monodromy test to identify and numerically characterize the monodromy based on the behavior of the closed orbits in the neighborhood of singular points or regions of the $\mathcal{EM}$ plane. This monodromy test can be performed systematically and does not require a deep mathematical knowledge of the equations of motion of the system. Furthermore, it can be easily implemented for different potentials to efficiently characterize the monodromy of a wide variety of systems. The validity of this monodromy test has been illustrated in the vicinity of the singular points in the (h, j) plane for several systems with azimuthal symmetry.

An interesting extension of this study covers the case of integrable systems with more degrees of freedom. It could also be of interest to extend these ideas to non-fully integrable systems. Of particular interests is the case of a rigid rotor interacting with an external field, such as the gravitational field. This kind of system is also interesting in molecular physics to model, for example, polyatomic molecules in combined parallel electric and nonresonant laser fields coupled to the polarizability[24,30,31] or THz laser fields coupled to the molecular hyperpolarizability.[32]

ACKNOWLEDGMENTS

J.J.O. acknowledges funding from the Juan de la Cierva-Incorporación program [Ministerio de Ciencia e Innovación (Spain)] and Project No. PID2019-106732GB-I00 (MINECO). R.G.-F. acknowledges financial support from Spanish Project No. FIS2017-89349-P (MINECO) and from the Andalusian research group FQM-207. This study has been partially financed by the Consejería de Conocimiento, Investigación y Universidad, Junta de Andalucía, and the European Regional Development Fund (ERDF) (Reference No. SOMM17/6105/UGR). R.G.-F. completed some of this work as a Fulbright fellow at ITAMP at Harvard University.

AUTHOR DECLARATIONS

Conflict of Interest

The authors have no conflicts to disclose.

DATA AVAILABILITY

The data that support the findings of this study are available from the corresponding author upon reasonable request.

APPENDIX A: THE SYMPLECTIC STRUCTURE

The space $\mathbb{R}^3 \times \mathbb{R}^3$ is endowed with the two-form

$$\omega = \sum_{i=1}^{3} \mathrm{d}x_i \wedge \mathrm{d}y_i.$$

The tangent bundle of the unit sphere

$$M = T\mathbb{S}^2 = \{(x,p) \in \mathbb{R}^3 \times \mathbb{R}^3 : \| x \| = 1, \langle x,p \rangle = 0\}$$

is a symplectic submanifold. This is automatic since the Poisson bracket of the constraints never vanishes.[27] Note that if $F_1(x,y) = \| x \|^2 - 1$, $F_2(x,y) = \langle x,y \rangle$, then

$$\{F_1, F_2\} = \sum_{i=1}^{3} \left\{ \frac{\partial F_1}{\partial x_i} \frac{\partial F_2}{\partial y_i} - \frac{\partial F_1}{\partial y_i} \frac{\partial F_2}{\partial x_i} \right\} = 2.$$

In M, we introduce the Lagrangian coordinates

$$\begin{cases} x_1 = \sin\theta\cos\varphi, \quad x_2 = \sin\theta\sin\varphi, \quad x_3 = \cos\theta, \\ y_1 = -\dot{\varphi}\sin\theta\sin\varphi + \dot{\theta}\cos\theta\cos\varphi, \\ y_2 = \dot{\varphi}\sin\theta\cos\varphi + \dot{\theta}\cos\theta\sin\varphi, \\ y_3 = -\dot{\theta}\sin\theta, \end{cases}$$

with $\theta \in [0,\pi]$ and $\varphi \equiv \varphi + 2\pi$.

The tangent planes at the north and south poles ($\theta = 0$ and $\theta = \pi$) are not covered by this chart. This will make some of our computations incomplete. The reader can easily fulfill the remaining details by using alternatives charts including these planes. After some computations, it can be seen that the form induced by ω on M is expressed as

$$\omega_M = \mathrm{d}\varphi \wedge \mathrm{d}p_\varphi + \mathrm{d}\theta \wedge \mathrm{d}p_\theta$$

with $p_\theta = \dot{\theta}$ and $p_\varphi = \dot{\varphi}\sin^2\theta$. We will employ the symplectic coordinates

$$q = \begin{pmatrix} \theta \\ \varphi \end{pmatrix}, \qquad p = \begin{pmatrix} p_\theta \\ p_\varphi \end{pmatrix}.$$

APPENDIX B: THE NUMERICAL PROCEDURE

The monodromy test requires the computation of the limits $\lim_{j\to 0^\pm}\chi(h,j)$ in Eq. (13) involving the integral in Eq. (14), which must be done numerically since, in general, it is not solvable analytically. This integral (13) is improper because it is finite although the integrand diverges in the upper and lower limits, i.e., $\sqrt{h - V_j(\alpha_\pm)} = 0$. This fact constitutes an obstacle for the numerical integration, which is bypassed following the procedure described in Ref. 33. First, the upper and lower limits, $\alpha_\pm$, are obtained by solving the equation $\sqrt{h - V_j(\alpha_\pm)} = 0$. The integral (13) is solved using the change of variables $x = \cos\theta$. The singularities in the upper and lower limits are treated as follows: (i) if the integrand $f(x)$ diverges as $(x-b)^{-\gamma}$, with $0 \le \gamma < 1$ and b being the upper limit, the singularities are removed by changing the variable $x = b - t^{\frac{1}{1-\gamma}}$ leading to

$$\int_a^b f(x)\mathrm{d}x = \frac{1}{1-\gamma}\int_0^{b-a^{1-\gamma}} t^{\frac{\gamma}{1-\gamma}} f\left(b - t^{\frac{1}{1-\gamma}}\right); \tag{B1}$$

(ii) if $f(x)$ diverges as $(x-a)^{-\gamma}$, with $0 \le \gamma < 1$ and a being the lower limit, the change of variable $x = a + t^{\frac{1}{1-\gamma}}$ results in

$$\int_a^b f(x)\mathrm{d}x = \frac{1}{1-\gamma}\int_0^{b-a^{1-\gamma}} t^{\frac{\gamma}{1-\gamma}} f\left(a + t^{\frac{1}{1-\gamma}}\right); \tag{B2}$$

and (iii) if $f(x)$ possesses singularities in both limits, as it occurs in the examples analyzed here, the integral is split and computed in the intervals $a \le x \le c$ and $c \le x \le b$, where $c \in (a,b)$ and $f(c)$ is well defined. Finally, the integrals (B1) and (B2) are evaluated.[33]

REFERENCES

[1] J. J. Duistermaat, Commun. Pure Appl. Math. **33**, 687 (1980).
[2] R. Cushman and J. J. Duistermaat, Bull. Am. Math. Soc. **19**, 475 (1988).
[3] B. Zhilinskii, J. Phys. A: Math. Theor. **43**, 434033 (2010).
[4] L. M. Bates, Z. Angew. Math. Phys. **42**, 837 (1991).
[5] N. J. Fitch, C. A. Weidner, L. P. Parazzoli, H. R. Dullin, and H. J. Lewandowski, Phys. Rev. Lett. **103**, 034301 (2009).
[6] J. B. Delos, G. Dhont, D. a. Sadovskií, and B. I. Zhilinskií, Europhys. Lett. **83**, 24003 (2008).
[7] C. Chen, M. Ivory, S. Aubin, and J. B. Delos, Phys. Rev. E **89**, 012919 (2014).
[8] M. P. Nerem, D. Salmon, S. Aubin, and J. B. Delos, Phys. Rev. Lett. **120**, 134301 (2018).
[9] D. A. Sadovskií and B. I. Zhilinskií, Mol. Phys. **104**, 2595 (2006).
[10] C. R. Schleif and J. B. Delos, Phys. Rev. A **76**, 13404 (2007).
[11] I. N. Kozin and R. M. Roberts, J. Chem. Phys. **118**, 10523 (2003).
[12] C. A. Arango, W. W. Kennerly, and G. S. Ezra, Chem. Phys. Lett. **392**, 486 (2004).
[13] G. Arwas and D. Cohen, Phys. Rev. A **99**, 023625 (2019).
[14] M. S. Child, T. Weston, and J. Tennyson, Mol. Phys. **96**, 371 (1999).
[15] M. Joyeux, D. A. Sadovskií, and J. Tennyson, Chem. Phys. Lett. **382**, 439 (2003).
[16] R. Cushman, H. R. Dullin, a. Giacobbe, D. Holm, M. Joyeux, P. Lynch, D. Sadovskií, and B. Zhilinskií, Phys. Rev. Lett. **93**, 024302 (2004).
[17] A. Giacobbe, R. H. Cushman, D. A. Sadovskií, and B. I. Zhilinskií, J. Math. Phys. **45**, 5076 (2004).
[18] B. P. Winnewisser, M. Winnewisser, I. R. Medvedev, M. Behnke, F. C. De Lucia, S. C. Ross, and J. Koput, Phys. Rev. Lett. **95**, 243002 (2005).
[19] N. F. Zobov, S. V. Shirin, O. L. Polyansky, J. Tennyson, P.-F. Coheur, P. F. Bernath, M. Carleer, and R. Colin, Chem. Phys. Lett. **414**, 193 (2005).
[20] C. Chen and J. B. Delos, Phys. Rev. E **97**, 062216 (2018).
[21] N. Martynchuk, H. W. Broer, and K. Efstathiou, Indagat. Math. **32**, 193 (2021).
[22] K. von Meyenn, Z. Phys. **231**, 154 (1970).
[23] B. Friedrich and D. Herschbach, J. Chem. Phys. **111**, 6157 (1999).
[24] J. H. Nielsen, H. Stapelfeldt, J. Küpper, B. Friedrich, J. J. Omiste, and R. González-Férez, Phys. Rev. Lett. **108**, 193001 (2012).
[25] K. Oda, M. Hita, S. Minemoto, and H. Sakai, Phys. Rev. Lett. **104**, 213901 (2010).
[26] V. I. Arnol'd, *Mathematical Methods of Classical Mechanics*, Graduate Texts in Mathematics Vol. 60 (Springer, New York, 1989).

[27]J. Moser and E. J. Zenhder, *Notes on Dynamical Systems* (American Mathemical Society, 2006), p. 192.
[28]R. Abraham, J. E. Marsden, and T. Ratiu, *Manifolds, Tensor Analysis, and Applications* (Springer, New York, 1988).
[29]*Dynamical Systems IV: Symplectic Geometry and its Applications*, Encyclopaedia of Mathematical Sciences, edited by V. Arnol'd and S. Novikov (Springer-Verlag, Berlin, Heidelberg; Moscow, 1990), p. 336.
[30]J. J. Omiste and R. González-Férez, Phys. Rev. A **86**, 043437 (2012).
[31]J. J. Omiste and R. González-Férez, Phys. Rev. A **88**, 033416 (2013).
[32]L. H. Coudert, J. Chem. Phys. **146**, 024303 (2017).
[33]W. H. Press, B. P. Flannery, S. A. Teukolsky, and W. T. Vetterling, *Numerical Recipes in FORTRAN 77: The Art of Scientific Computing*, 2nd ed. (Cambridge University Press, 1992).